SolarPACES 2022, 28th International Conference on Concentrating Solar Power and Chemical Energy Systems
Receivers and Heat Transfer Media and Transport: Point Focus Systems
https://doi.org/10.52825/solarpaces.v1i.728

Published: 26 Jan. 2024

Design and Construction of a 700kW$_{th}$ High-Temperature Sodium Receiver

Joe Coventry[1][https://orcid.org/0000-0003-4020-3980], Felix Venn[1], Daniel Potter[2], Charles-Alexis Asselineau[1][https://orcid.org/0000-0002-3750-5737], Wilson Gardner[2][https://orcid.org/0000-0002-2663-1746], Jin-Soo Kim[2], William R. Logie[1][https://orcid.org/0000-0003-0184-1816], Robbie McNaughton[2][https://orcid.org/0000-0002-3788-6824], John Pye[1][https://orcid.org/ 0000-0001-8026-0045], and Wesley Stein[2]

[1] School of Engineering, Australian National University, Canberra, Australia.

[2] CSIRO Energy, Newcastle, New South Wales, Australia

Abstract. The Australian Solar Thermal Research Institute (ASTRI) has been developing technologies designed to collect and store solar energy at high-temperature to drive a new high-efficiency power block based on the supercritical CO_2 Brayton cycle. ASTRI is pursuing two alternative pathways: one based on the use of liquid sodium as a heat transfer fluid, and the other based on the use of solid particles. The current work describes ASTRI's progress towards design and construction of a 700kW$_{th}$ prototype sodium receiver suited to this type of system, which will be installed and tested on Solar Field 2 at the CSIRO Energy Centre in Newcastle, Australia. The receiver is a cavity receiver with a circular aperture oriented at a tilt down towards the centre of the heliostat field. Inside the cavity are ten vertical tube banks in a semi-circular arrangement, with sodium flowing from the centre to the outside in a serpentine manner. Optical and thermal modelling at design point predicts aperture interception efficiency of 95.3%, receiver efficiency of 90.9% and thus a combined interception and receiver efficiency of 86.6%. Conservative flux limits are set based on the tube material's (Alloy 625) time independent tensile strength, which is dominated by creep for the sodium temperatures considered. In the event of incident, the receiver is designed to drain and a door closes over the aperture to limit smoke egress. Insulation is SiO_2-CaO-MgO blanket, and all pipes are heat traced. Fabrication of the receiver was completed in July 2022 and first on-sun testing is expected in September 2023.

Keywords: Sodium, Receiver, CSP, Concentrating Solar, Prototype

1. Introduction

The Australian Solar Thermal Research Institute (ASTRI) has been developing technologies designed to collect and store solar energy at high-temperature to drive a new high-efficiency power block based on the supercritical CO_2 Brayton cycle [1]. This work is closely aligned to international research efforts, in particular the U.S. Gen3 CSP program [2]. In this program, a turbine inlet temperature of 700°C was set, well above the stability limit of conventional heat transfer and storage media used in state-of-the-art concentrating solar power (CSP) plants. ASTRI is pursuing two alternative pathways compatible with these high temperature requirements: one based on the use of liquid sodium as a heat transfer fluid, and the other based on the use of solid particles. The current work describes ASTRI's progress towards design and construction of a 700 kW$_{th}$ prototype sodium receiver, which will be installed and tested on Solar Field 2 at the CSIRO Energy Centre in Newcastle, Australia.

Development and testing of sodium receiver technologies dates back to 1980s, including a series of tests at Sandia National Laboratories in the U.S. [3] and at the Plataforma Solar in

Almeria, Spain [4]. Overall, the outcomes from these tests were highly positive, with excellent thermal efficiency results and development of significant operational experience [5]. Over the past decade, Australian company Vast Solar has further developed sodium receivers for deployment in a modular, multi-tower CSP configuration [6]. However, these receivers were designed for maximum temperatures around 520-560°C. Delivery of heat to a turbine at 700°C requires a major step up in the upper receiver temperature, and hence a significant re-assessment of the design.

2. Concept design

2.1 Design criteria

To meet ASTRI's objective to further the development and demonstration of next generation, higher temperature solar thermal technologies, and to align with the requirements of the US Generation 3 CSP program (in particular the Liquid Pathway project [2]) the operational temperature range for the sodium receiver was set to 520-740°C. As this will be a first-of-a-kind demonstration of a sodium receiver at this high temperature range, the highest priority in design was given to safety and ensuring successful demonstration of operation. However, this priority was not set completely at the expense of performance. Sodium is often discussed as beneficial for receiver performance in comparison to other fluids [7], in particular because high thermal conductivity reduces the front-to-back receiver tube temperature and associated thermal stresses, and therefore allows higher solar fluxes and more compact receiver designs. This provides the potential to reduce both thermal losses and capital cost. Therefore the design criteria established included both these factors, along with several others as listed below.

- Demonstrate the successful operation and integration of a 700kW_{th} sodium cavity receiver
- Design and test a receiver to match expected operating conditions for a commercial plant featuring a supercritical CO_2 power cycle
- Demonstrate a design that is simple, scalable, and durable, supporting the objective of lowering the cost of CSP
- Validate receiver performance models using experimental data
- Increase understanding of receiver design interfaces with system balance of plant
- Demonstrate a receiver efficiency greater than 86%

2.2 Concept design development

Two cavity-type receiver concepts were initially evaluated by ASTRI. Inspired by the SG4 dish receiver [8], the first of these was based on a deep cylindrical/conical type design, with surrounding spillage skirt and a "ribcage"-like flow path to allow drainage [9]. The second was based on a concave-tube-bank-in-cavity concept, with similar overall geometry to the CO_2 receiver developed by Abengoa, and tested previously at CSIRO [10]. While the first of these two designs was evaluated to have potential performance advantages, the simplicity and scale-up feasibility of the second concept were decisive factors in its down-selection for further development.

Potter et al. [11] describe the concept performance modelling process for this design, in which ray tracing and heat transfer modelling were implemented using CSIRO's Heliosim software. The initial design was a tilted cavity, with both the circular aperture and banks of tubes angled down towards the heliostat field. However, in a further iteration, the tube banks were reoriented vertically to simplify their mounting (on spring hangers), and to reduce the likelihood of sodium egress from the aperture in the event of a sodium leak. Heliostats aim at the centre of the aperture, with different combinations of heliostats from CSIRO Solar Field 2 selected depending on the sun position to maintain the 700 kW design output (where possible), while also trying to maximise receiver efficiency and respect flux limits (discussed further below).

The final receiver geometry from the conceptual design phase is shown in Figure 1, also showing the predicted absorbed flux at design point (equinox solar noon). There are 10 tube banks, each consisting of 7 seam welded tubes, 25.4 mm × 1.65 mm minimum wall thickness, from Alloy 625 (UNS NO6625) Grade 2 material split into left and right sections. Two separate fluid supply lines (with separate pumps) introduce sodium to the two banks at the centre of the receiver, and then fluid flows in a serpentine manner through the tube banks to the outside. In this way the highest flux region corresponds the coldest fluid region. Table 1 details the tube and flow path design. Figure 2 has key dimensions. Performance parameters simulated at design point are listed in Table 2.

Table 1. Details of the tube, tube bank spacing, layout and flow path for the conceptual receiver design.

Item	Unit	Value
Receiver tube outer diameter	mm	25.4
Receiver tube separation	mm	0.7
Receiver tube count per tube bank		7
Tube banks per flow path		5
Flow paths		2
Relative azimuth angle between adjacent tube banks	degrees	12
Irradiated length per pipe	mm	1300

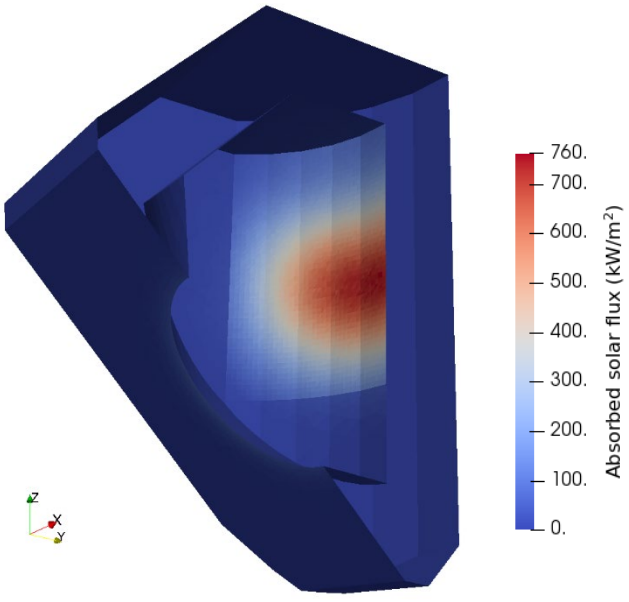

Figure 1. Heliosim 3D surface model of the conceptual receiver design, with a section mid receiver showing the predicted absorbed solar flux at design point.

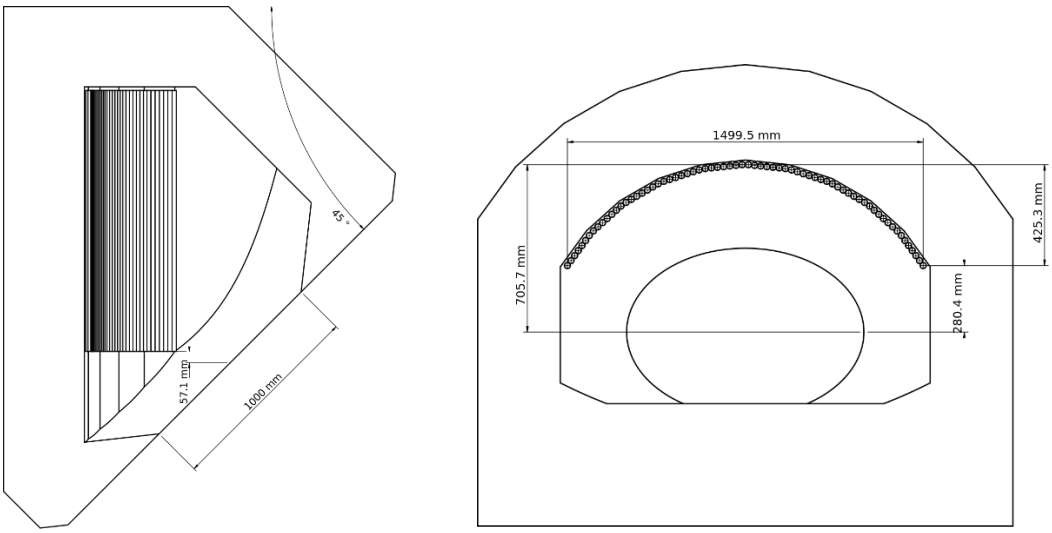

Figure 2. Overall dimensions of the conceptual receiver design, showing cross section from west (left) and above (right).

Table 2. Design point conditions and performance for the ASTRI 700 kW_{th} sodium receiver concept design.

Item	Unit	Value
DNI (W/m^2)	W/m^2	900
Installed heliostats (CSIRO Field 2)		396
Available heliostats		235
Utilised heliostats		235
Power through aperture	kW	782
Spillage loss	kW	38.5
Receiver solar reflection loss	kW	16.5
Receiver thermal radiation loss	kW	33.1
Receiver convection loss	kW	15.5
Receiver conduction loss	kW	6.4
HTF thermal output	kW	711
Aperture interception efficiency	%	95.3
Receiver efficiency	%	90.9
Combined interception and receiver efficiency	%	86.6
East flow path average mass flow rate per pipe	kg/s	0.183
West flow path average mass flow rate per pipe	kg/s	0.183
East flow path peak fraction of allowable net flux		0.955
West flow path peak fraction of allowable net flux		0.934
Peak insulation behind pipes surface temperature	°C	806
Peak shield surface temperature	°C	1116
Peak insulation surface temperature	°C	928
Peak pipes back surface temperature	°C	748
Peak pipes front surface temperature	°C	789
Peak average pipe wall temperature	°C	743
Peak temperature disparity across pipes in a single panel	°C	13.9
Peak sodium outlet temperature disparity	°C	16.8
Peak sodium temperature	°C	748

2.3 Structural integrity analysis

Initial design screening used a reduced 2D generalised plane strain analytical model implemented in Python *nashTubeStress* [12] to evaluate the risk of excessive deformation (plastic), thermal ratcheting (cyclic incremental plastic deformation), and adherence to the linear elastic material strength limits dictated by creep-rupture data. Flux limit tables derived from thermoelastic-stress were generated for the range of metal temperatures expected on the prototype receiver, specific to its flow conditions and tube dimensions.

As the design developed, a more detailed 3D Finite Element Analysis (FEA) evaluation was developed to include tube banks, their connection via headers to interconnect piping, and the overall structural fixture of panels to framework. Stresses considered were primary stresses due to internal pressure (200 kPa gauge) and dead-weight (vessel and contents), and secondary stresses resulting from thermal expansion under live loads (temperature and flux). Two nickel-based superalloy tubing materials were considered for fabrication of the prototype receiver: 25:4 mm OD x 1:65 mm WT Alloy 625 (UNS N06625) and 33:4 mm OD x 1:32 mm WT Alloy230 (UNS N06230). Due to sourcing restrictions, solution annealed (Grade 2) Alloy 625 was chosen despite Alloy 230 being preferable (due to lower thermal stresses and lower susceptibility to over-ageing). Figure 3a shows design tensile strength *f*-values derived from manufacturer data-sheets for Alloy 625 alongside values given for allowable stress intensity S_m and yield strength S_y from ASME BPVC II, Part D, Table 1B–2010, based on:

- stress to cause rupture in time t at design temperature S_{Rt} divided by 1.5;
- yield strength at design temperature R_{eT} divided by 1.5; and
- ultimate tensile strength at design temperature R_{mT} divided by 3.5.

The lowest curve of this combination of limits was used to construct the time-dependent design tensile strength or *f*-value curves in time t. Given the range of bulk sodium temperature being considered for this technology it can already be observed that the design tensile strength *f*-values will be governed by creep. Applying the design tensile strength at temperature to the design point conditions of a particular tubing product results in a specific peak allowable net flux. Figure 3b shows this for time independent design tensile strength (the lower curve) and time-dependent *f*-values derived from manufacturer's data-sheets. Given the short duration of the planned test program, the flux limits for the prototype receiver were set based on creep-rupture lifetime of 1000 h (the orange curve in Figure 3b). More aggressive flux limits and longer lifetimes, including up to the typical 30 year design life of a CSP plant, are feasible at this temperature range, as was demonstrated in the analysis carried out as part of the Gen3 CSP Liquids Pathway project [2]. However sourcing suitable materials (e.g. Alloy 740H) and carrying out the necessary inelastic thermo-mechanical analysis was not feasible within the budget and time constraints of this project.

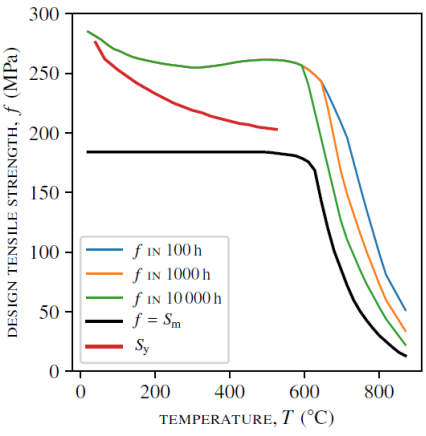

(a)

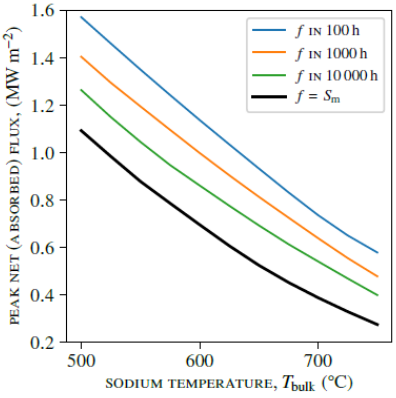

(b)

Figure 3. (a) Design tensile stress *f* for Alloy 625 showing time-dependent values derived from manufacturer's data compared to time-independent (S_m) allowable stress values from ASME BPVC II, Part D. (b) Peak allowable net flux (that which is absorbed by the tube, not including loss to ambient via radiation and convection) for UNS N06625 using creep-rupture data from manufacturer's data-sheets and ASME allowables for a mass flow of 0.18 kg s^{-1}.

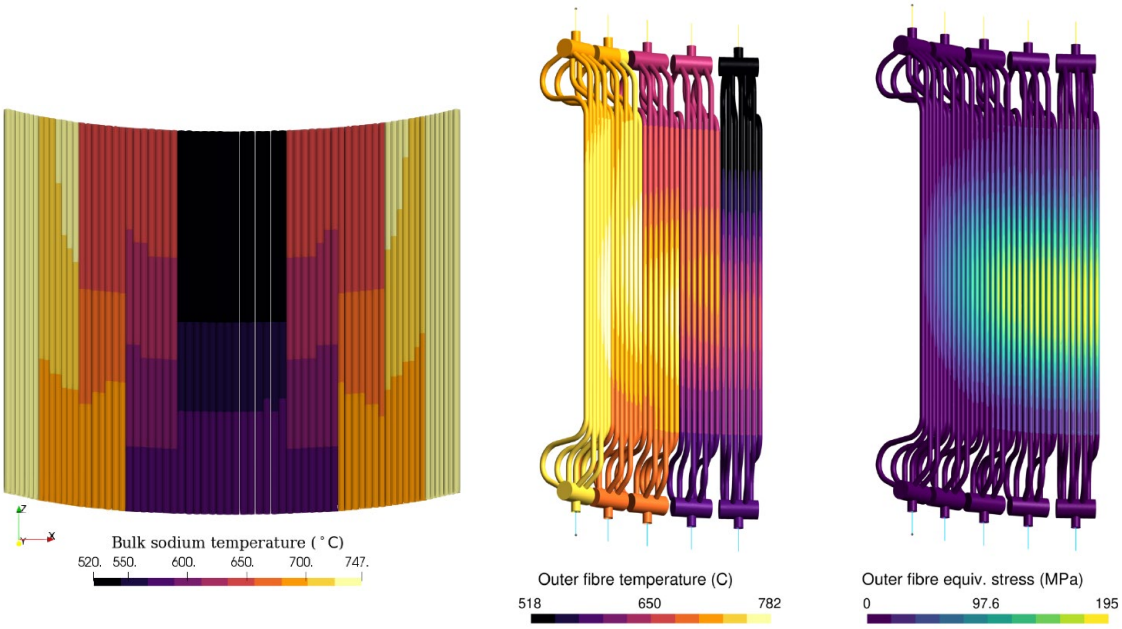

(a) (b) (c)

Figure 4. (a) Bulk sodium temperature distribution, (b) outer fibre temperature, and (c) outer fibre equivalent stress at design point (equinox solar noon).

Figure 4a shows the bulk fluid temperature entering east and west flow paths in the middle from the top and continuing in panels of seven tubes towards the left and right outer edge in a serpentine fashion. Fluid temperature is raised from the inlet at 520°C to a maximum of 747°C at the outlet by the net absorbed flux, as shown in Figure 4b. The highest flux absorbed is 0.76 MWm^{-2} on the 5th tube of the first panel of the east flow-path (i.e. near the centre of the receiver). The bulk sodium temperature at this point is 555°C and the maximum surface temperature is 668°C. Assuming constant material properties for UNS N06625 at 650°C in *nashTubeStress* with a net absorbed flux of 0.76 MWm^{-2} results in an outer fibre equivalent (von Mises) stress of 262 MPa. A 2D generalised plane strain FEA model of the same point with temperature dependent mechanical properties results in reduced stress of 255 MPa. However, the generalised plane strain 3D panel model and analysis also incorporates the headers and tube bends, which act like springs to allow bending, so that despite the assumption of generalised plane strain at the junction to the interconnect piping, the resulting peak outer fibre equivalent stress of 195 MPa is significantly lower than that calculated for 2D generalised plane strain tubes (Figure 4c).

3. Detailed design

With the concept design established, the detailed design phase commenced. Apart from the tube-banks themselves, the receiver consists of a receiver frame and cladding, a panel mounting system (on spring hangers), instrumentation (thermcouples), a mechanical door, a spill tray, interconnecting piping including fill and drain lines and valves, heat tracing, and insulation. The cavity was enlarged slightly from the conceptual design to accomodate increased inter-tube-bank spacing and the spill tray. In addition, as a result of recommendations from a Hazard and

Operability (HAZOP) study, thermal cameras were added to monitor front-side tube temperature.

3.1 Design standards

The receiver was designed in accordance with Australian Standard AS1210 2010 Class 1. Structural consultants *FE Consultants* were engaged to assist in the detailed design phase, to help with code interpretation, review the design by analysis techniques and compliance with standards for all the relevant load cases and assessment criteria, and to complete the detailed design drawings. A commercial, finite element code (Abaqus 2020) was used, with stress analysis now incorporating the interconnecting pipework and panel support sytem. The consultants concluded that the sodium receiver and piping design compied with AS1210 and sound engineering practice. Some of the design details are listed below:

- Operating pressure is 200 kPa (gauge) and design pressure 300 kPa (gauge).
- Hydrostatically testing was carried out in accordance with AS1210-2010 at 760 kPa (gauge).
- Creep design life is 1000 h and number of design thermal cycles is 500, although it is noted that the potential operating life is expected to be between 10,000 and 100,000 hours.
- The design low cycle temperature is 300°C, noting the intention is to maintain this temperature during the night and non-operational periods during testing campaigns, to minimise the ingress of impurities during the draining and filling process.
- The pressure related hazard level level according to AS4343 is C (low pressure)
- Total sodium volume in the receiver is approximately 85 L.
- Post weld heat treatment is not required. However, a post bending anneal was specified for interconnect piping bends with a strain rate >15% as per the material manufacturer's guidelines
- Top headers were supported via a dummy leg, supported by spring hangers

Bends at the ends of the receiver tubes allow for deflections, essential for stress relief given flux and tube temperature variation across individual panels. The tubes are bent in an alternating fashion (refer to Figure 5) to allow enough spacing for the butt welds of the tubes to the headers. Interconnecting piping is also designed with sufficient length and bends to cope with thermal expansion mismatch between tube banks, in accordance with AS1210 and ASME B31.3. The receiver is designed with drain and fill lines that allow sodium to fill from the bottom in normal operation, pushing the cover gas (argon) up and out through the vent lines. The valves on these lines are closed in operation, but fail open so that in the event of incident, the receiver would completely drain, with sodium returning to the drain tank in the main sodium loop.

Figure 6a shows the final design, which includes a door that can be closed when the receiver is either not in use or is in warm standby, or automatically closes (assisted by a counterweight) in the event of tube failure during operation to minimise smoke egress. Seals around the door, combined with water shedding features on the receiver enclosure, prevent water from entering the enclosure. Figure 6b shows a section view with the door removed to show the aperture position relative to the tube bank. A drip tray at the base of the cavity space drains to a sealed plenum area, capable of containg the entire inventory of sodium from the receiver in case of tube rupture. The receiver enclosure is connected via a vent line (with an actuated valve) to the main sodium loop enclosure, which would allow smoke to be drawn into the scrubber system in the event of a sodium leak. The receiver tubes are painted with the absorber coating Pyromark 2500, generally following the procedure outlined by Ho et al.[13], although the final curing step is at 700°C to avoid unnecessarily rapid aging/degradation of the coating that occurs at higher temperatures [14].

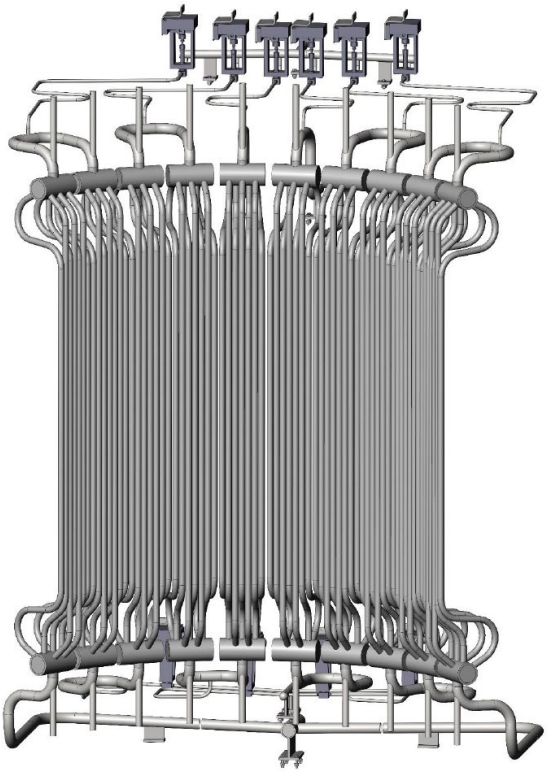

Figure 5. 3D model of the sodium receiver showing the tube bank arrangement, including the drain and fill lines.

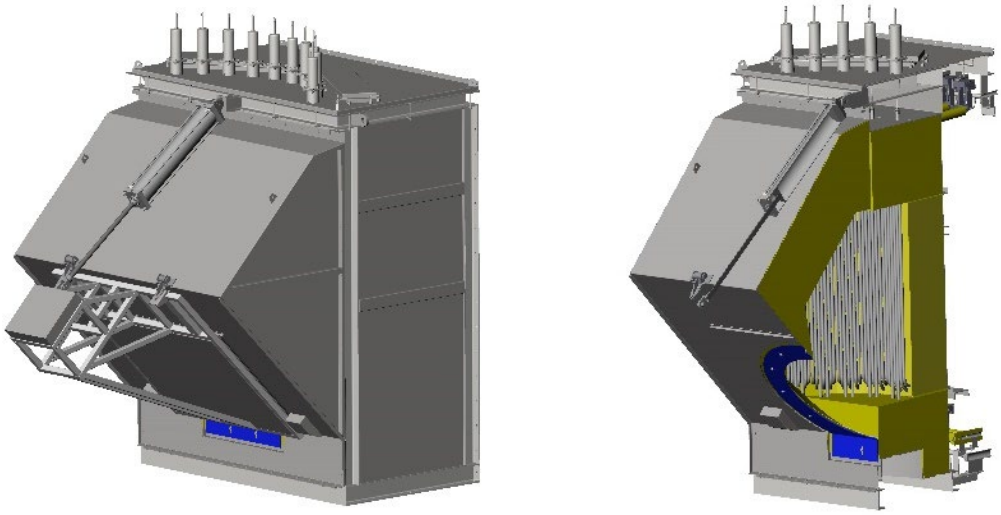

(a) (b)

Figure 6. 3D models of the sodium receiver showing (a) the full receiver, including the door in the closed position, and (b) a section view through the centre of the receiver, with the door removed to show the aperture.

Instrumentation includes 32 Type-K stainless steel sheathed thermocouples clamped to the backs of the tubes. Most of these are located along the horizontal centreline of the receiver, at the left- and right-most tubes of each panel (i.e. 20 in total). Two of the panels (one at the centre, one at the edge) are more densely instrumented, with additional thermocouples located along the centreline, and at locations on the tube bends at the top and bottom. A further 35 thermocouples are located on interconnecting pipework, drain and vent lines, and both inside and outside the insulation at various locations around the enclosure. Tube temperature on the

front side will be monitored by two thermal cameras mounted on supports cantilevered in front and below the receiver.

The insulation is SiO_2-CaO-MgO (Superwool Plus) blanket, pinned in layers to the inside of the housing. The thickness and blanket density (either 96 or 128 kg/m^3) varies depending on location, for example, 525 mm at the top, 225 mm at the front around the aperture, 350 mm on the sides, 50 mm on the door, and 450 mm behind the tubes at the back. At the rear, the insulation and housing are arranged in removable “plugs“ to improve access to this region. Total mass of insulation on the receiver is 666 kg. All pipework except the receiver tubes themselves are installed with heat tracing (HTS/Amptek Heavy Insulated Duo-Tape), to ensure sodium can fill the loop without blockage. Heating the receiver tubes will be done with solar flux from the heliostat field.

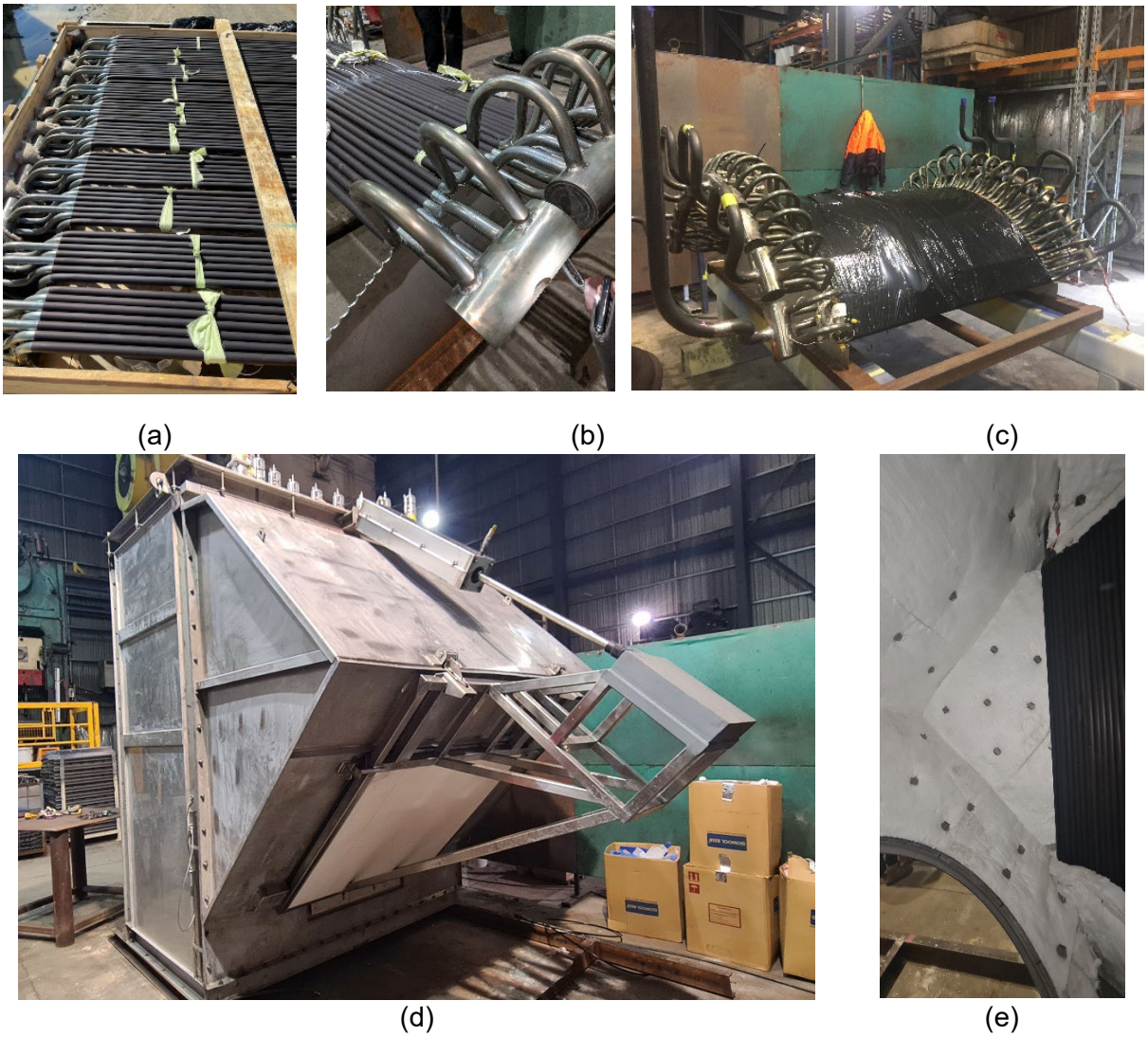

Figure 7. The sodium receiver in various stages of construction showing (a,b) the completed tube banks, (c) the tube banks welded to the interconnecting piping, (d) the competed receiver enclosure with door and (e) a view from inside the receiver showing the insulation.

4. Construction

The receiver tubes were bent and welded to the headers to form the tube banks by MCM Manufacturing in Newcastle. They were then painted with the Pyromark 2500 absorber coating, and transferred to Performance Engineering Group. There the receiver enclosure and door were fabricated, and the tube banks mounted within along with interconnecting pipework

and valves. Acceptance testing included standard procedures such as hydrostatic testing, non-destructive testing of welds (100% RT of pipe butt welds, and 100% DPI of non-butt welds), as well as a water ingress test to confirm the enclosure and door were adequately water tight. The key challenge during construction related to welding of the Alloy 625 material, which is not a simple material to weld. Weld rectification work was required for many of the welds in order to pass the NDT requirements. Another challenge was sourcing of Alloy 625 grade 2 in the small quantities required for the prototype. For the 25.4mm diameter tubing, seam-welded material was able to be sourced. It is noted that the tube bank manufacturer measured the thickness of the tubing to be approximately 2.4mm, which is outside the tolerance for minimum wall thickness tubing (+28 / -0%). However, due to the sourcing challenges, this material was used for fabrication of the tube banks. Figure 7 shows some images of the receiver at various stages of fabrication.

Figure 8. The receiver and sodium loop mounted on a skid, on route from the fabricator in Newcastle to Vast Solar's Jemalong site for sodium fill and on-ground commissioning steps.

5. Conclusion

Fabrication of the receiver was completed in July 2022. The receiver is designed to interface with a new sodium loop at CSIRO Newcastle, as described by Gardner et al. [15] in a companion paper. The receiver has been assembled on a skid with the sodium loop, and in May 2023 was sent to Vast Solar's Jemalong site for the ground (off-sun) commissioning steps, including the sodium fill and the operational safety testing program (Figure 8). Subsequently, the skid will be returned to Newcastle, then lifted onto the tower in Field 2 for the on-sun testing campaign, which is expected to commence in September 2023.

Data availability statement

Data is not presented in this article. Further information about the receiver design and construction is available upon request.

Author contributions

Joe Coventry: Conceptualisation, Formal Analysis, Investigation, Writing – Original Draft, Project administration, Supervision, Funding acquisition, Felix Venn: Conceptualisation, Methodology, Formal analysis, Investigation, Visualisation, Daniel Potter: Conceptualisation, Methodology, Software, Formal analysis, Visualisation, Charles-Alexis Asselineau: Conceptualisation, Methodology, Software, Formal analysis, Visualisation, Wilson Gardner: Conceptualisation, Investigation, Jin-Soo Kim: Conceptualisation, Investigation, Supervision, William R. Logie: Methodology, Software, Formal Analysis, Robbie McNaughton: Conceptualisation, Investigation, John Pye: Conceptualisation, Formal Analysis, Investigation, Supervision, Wesley Stein: Conceptualisation, Supervision, Project Administration, Funding acquisition.

Competing interests

The authors declare no competing interests.

Funding

This research was performed as part of the Australian Solar Thermal Research Institute (ASTRI), a project supported by the Australian Government, through the Australian Renewable Energy Agency (ARENA).

Acknowledgement

The authors would like to acknowledge and thank Byron Laird and the team at FE Consultants, who provided invaluable assistance during the detailed design stage, and Ildo Agnetti and the team at John Cockerill for invaluable advice during the concept design. The authors also wish to acknowledge the huge efforts and support by the teams at Performance Engineering Group and MCM Manufacturing during the receiver fabrication.

References

1. J. Coventry *et al.*, “Development of ASTRI high-temperature solar receivers,” presented at the SOLARPACES 2016: International Conference on Concentrating Solar Power and Chemical Energy Systems, Abu Dhabi, United Arab Emirates, 2017, p. 030011. doi: 10.1063/1.4984354.
2. C. S. Turchi *et al.*, “CSP Gen3: Liquid-Phase Pathway to SunShot,” United States, NREL/TP-5700-79323, 2021. Online.. Available: https://doi.org/10.2172/1807668
3. Rockwell International, “Sodium solar receiver experiment. Final report,” SAND82-8192, Dec. 1983. doi: https://doi.org/10.2172/5332177.
4. P. Kesselring and Clifford S Selvage, Eds., *The IEA, SSPS Solar Thermal Power Plants - Facts and Figures - Final Report of the International Test and Evaluation Team (ITET): Volume 1: Central Receiver System (CRS)*. Berlin Heidelberg: Springer, 1986.
5. J. Coventry, C. Andraka, J. Pye, M. Blanco, and J. Fisher, “A review of sodium receiver technologies for central receiver solar power plants,” *Sol. Energy*, vol. 122, pp. 749–762, Dec. 2015, doi: https://doi.org/10.1016/j.solener.2015.09.023.
6. B. Leslie and K. Drewes, “Holistic optimisation of modular field design including heliostats, receivers, towers, HTF piping and operations,” presented at the SOLARPACES 2020: International Conference on Concentrating Solar Power and Chemical Energy Systems, Freiburg, Germany, 2022, p. 120016. doi: https://doi.org/10.1063/5.0089018.

7. C. K. Ho and B. D. Iverson, “Review of high-temperature central receiver designs for concentrating solar power,” *Renew. Sustain. Energy Rev.*, vol. 29, no. 0, pp. 835–846, 2014, doi: https://doi.org/10.1016/j.rser.2013.08.099.
8. J. Pye *et al.*, “Experimental Testing of a High-Flux Cavity Receiver,” presented at the SOLARPACES 2016: International Conference on Concentrating Solar Power and Chemical Energy Systems, Abu Dhabi, United Arab Emirates, 2016. doi: doi.org/10.1063/1.4984485.
9. C.-A. Asselineau *et al.*, “Design of ASTRI’s high-temperature liquid sodium receiver prototype,” presented at the SOLARPACES 2019: International Conference on Concentrating Solar Power and Chemical Energy Systems, 2019. doi: https://doi.org/10.13140/RG.2.2.29674.95680.
10. Y. C. Soo Too, M. Diago López, H. Cassard, G. Duffy, R. Benito, and R. Navio, “Thermal Performance and Operation of a Solar Tubular Receiver With CO2 as the Heat Transfer Fluid,” *J. Sol. Energy Eng.*, vol. 139, no. 4, 2017, doi: https://doi.org/10.1115/1.4036414.
11. D. Potter, J.-S. Kim, and R. McNaughton, “Simulation of a demonstration high temperature liquid sodium receiver with Heliosim,” presented at the Asia-Pacific Solar Research Conference, Canberra, 2019.
12. W. R. Logie, J. D. Pye, and J. Coventry, “Thermoelastic stress in concentrating solar receiver tubes: A retrospect on stress analysis methodology, and comparison of salt and sodium,” *Sol. Energy*, vol. 160, pp. 368–379, Jan. 2018, doi: https://doi.org/10.1016/j.solener.2017.12.003.
13. C. K. Ho, A. R. Mahoney, A. Ambrosini, M. Bencomo, A. Hall, and T. N. Lambert, “Characterization of Pyromark 2500 for High-Temperature Solar Receivers,” presented at the ASME 2012 6th International Conference on Energy Sustainability, San Diego, 2012. doi: doi.org/10.1115/ES2012-91374.
14. S. Hosseini, J. F. Torres, M. Taheri, A. Tricoli, W. Lipiński, and J. Coventry, “Long-term thermal stability and failure mechanisms of Pyromark 2500 for high-temperature solar thermal receivers,” *Sol. Energy Mater. Sol. Cells*, vol. 246, p. 111898, Oct. 2022, doi: https://doi.org/10.1016/j.solmat.2022.111898.
15. W. Gardner *et al.*, “Design and construction of a high-temperature solar sodium test facility,” presented at the SOLARPACES 2022: International Conference on Concentrating Solar Power and Chemical Energy Systems, Albuquerque, 2022.